Acta Mech 227, 3295–3303 (2016)
DOI 10.1007/s00707-015-1544-7

ORIGINAL PAPER

Richard Wendler · Williams R. Calderón-Muñoz · Richard LeBoeuf

Energy-based iteration scheme of the double-multiple streamtube model in vertical-axis wind turbines

Received: 31 December 2014 / Published online: 23 January 2016

Abstract Due to their simplicity, blade element momentum models, such as the double-multiple streamtube (DMS) model, are among the most common models to predict the performance of Darrieus vertical-axis wind turbines (VAWTs). A two-dimensional energy-based iteration scheme of the DMS model (EB-DMSM) is shown in the present work. Its purpose is to improve predictions of power performance and flow expansion. This new approach is compared with a momentum-based iteration scheme (MB-DMSM) and the results of a two-dimensional computational simulation of a 12-kW straight-bladed VAWT. The mathematical representation of streamlines used for modeling the flow expansion is in good agreement with the simulations. Convergence of both schemes is achieved for tip-speed ratios (TSRs) up to 4. Failure of the models to convergence at higher TSRs is attributed to their inability to adequately represent the aerodynamic forces acting on the blades, due to the simplicity of their formulation. Relative to computational simulations, the maximum differences in the peak power coefficient predictions are 16 and 32 % and in the flow expansion predictions are 53 and 5 % for the MB-DMSM and EB-DMSM, respectively. Corrections are required to improve predictions of power performance and flow expansion of turbines with different geometric and operational parameters.

1 Introduction

Interest in Darrieus VAWTs has increased in recent years [1,2], due in part to the potential of this technology to be used in urban environments in the small scale [3,4]. The vertical axis of these turbines allows them to be omnidirectional and to be installed with the generator at the level of the ground or rooftop [4]. Therefore, they are considered versatile designs that can have lower capital, operating and maintenance costs. Additionally, for the same nominal power, the rotational speeds are lower for a Darrieus VAWT than for a horizontal-axis wind turbine (HAWT) [5]. Thus, Darrieus VAWTs have fewer vibrations and make less noise than HAWTs. In addition to being urban friendly, recent studies show that wind farms of Darrieus VAWTs can have a higher power density than HAWTs [6–10]. This could be advantageous in the medium and large scale.

R. Wendler · W. R. Calderón-Muñoz (✉)
Department of Mechanical Engineering, Universidad de Chile, Beauchef 851, Santiago, Chile
E-mail: wicalder@ing.uchile.cl
Tel.: +56-2-29784469
Fax: +56-2-26988453

W. R. Calderón-Muñoz
Energy Center, Universidad de Chile, Tupper 2007, Santiago, Chile

R. LeBoeuf
Facultad de Ingeniería y Ciencias Aplicadas, Universidad de los Andes, Monseñor Álvaro del Portillo, 12455 Las Condes, Santiago, Chile

Due to the variety of possible operating conditions, a low-cost computational tool, which provides a fast and relatively accurate prediction of power performance, would be useful for optimizing the use of VAWTs. Blade element momentum (BEM) models, especially double-multiple streamtube (DMS) models, provide good estimations of the power performance of wind turbines [11]. Variations of the wind resource present in urban environments and wind farms can be modeled as an inlet condition (wind profile) in two-dimensional BEM models. Boundary layer effects and blade tip losses can be included to model a three-dimensional turbine. Note that the two-dimensional DMS model, which corresponds to straight-bladed turbines, can be easily modified for other geometries such as helical-bladed turbines. Other semi-analytical models such as the vortex model shown in [12] have the advantage of being more accurate in the prediction of power performance and description of the unsteady flow around the turbine, but they have the disadvantage of requiring considerably more computational resources and time than BEM models.

The purpose of this work is to formulate and study the behavior of an energy-based iteration scheme of a DMS model that takes into account flow expansion. Note that the energy-based iteration scheme is equivalent to the momentum-based iteration scheme for a one-dimensional, frictionless, steady flow model. The main difference is in the use of tangential force coefficients rather than streamwise force coefficients. The basic DMS models used in [11,13] do not take into account flow expansion. A DMS model that takes into account flow expansion was developed in [14]. However, the models are known to have convergence problems at high turbine solidities and high turbine-load states [15]. The momentum-based iteration scheme, MB-DMSM, and the energy-based iteration scheme of the DMS model, EB-DMSM, are quasi two-dimensional, because the models are based on a one-dimensional theory, but the use of multiple streamtubes in the cross-flow direction models the lateral expansion of the flow.

2 Computational simulations

An unsteady two-dimensional CFD simulation was performed using the finite volume method implemented in ANSYS Fluent 13.0.0. The turbine geometry was based on a 12-kW SB-VAWT [16]. It has three 0.25-m chord NACA 0021 airfoil blades, a diameter of 6 m, a solidity of 0.25 and a tower diameter of 0.2 m.

The computational domain shown in Fig. 1, including boundary conditions, is similar to previous works [17–19]. It is 5 turbine diameters wide and 14.5 turbine diameters long. A sliding mesh technique is used in order to have a rotational sub-domain inside the static domain. The rotational domain, which includes the turbine blades and the central tower, has a diameter equal to 4/3 the turbine diameter.

ANSYS Meshing is used to produce the mesh, which is unstructured and contains only triangular elements, as shown in Fig. 2. The rotational domain is refined in order to get high resolution of shed vortices and other wake effects. In order to reduce error in calculations of aerodynamic forces and moments, the area around the airfoil is refined even further, as shown in Fig. 2. A summary of the most important mesh metrics is shown in Table 1; both skewness and orthogonal quality metrics are within expected ranges (skewness $\leq$0.8 and orthogonal quality $\geq$0.2).

Results from steady-state simulations of a stationary turbine are used as initial conditions of the transient simulations. The pressure-velocity coupling method used for the steady-state simulation is the semi-implicit method for pressure-linked equations (SIMPLE), and for the transient simulations, it is the pressure-implicit

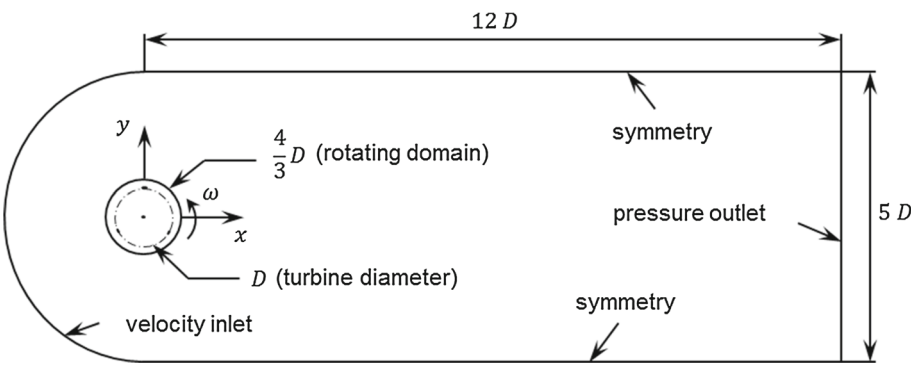

Fig. 1 Computational domain of the two-dimensional CFD simulations

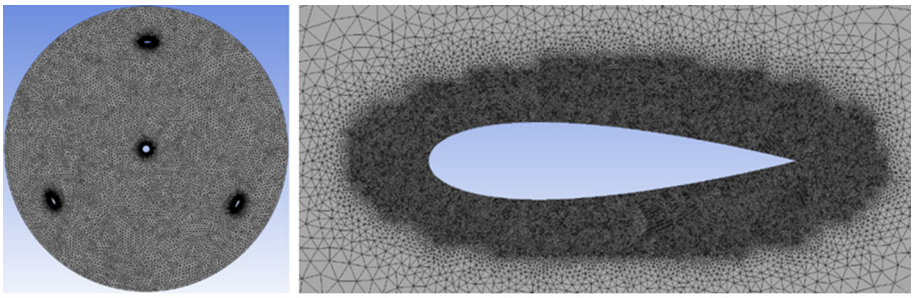

Fig. 2 **a** Detail view of the mesh of the rotating domain **b** mesh element sizing near a blade

Table 1 Mesh metrics

Metric	Value
Number of elements	550,881
Number of nodes	277,490
Skewness (maximum)	0.74
Skewness (average)	0.062
Orthogonal quality (minimum)	0.472
Orthogonal quality (average)	0.96
Courant number at interface	0.35
Average $y+$ at blade surface	30

method with splitting of operators (PISO) [20]. The $k-\omega$ SST (shear stress transport) turbulence model and an enhanced wall treatment are used [21]. Average $y+$ values around the blades are approximately 30, which is appropriate for the enhanced wall treatment formulation [22]. First-order spatial discretization was used during the steady-state simulations for pressure, momentum, turbulent kinetic energy, turbulent dissipation rate and energy variables. The same variables are discretized using second-order discretization during the transient simulations, in order to obtain a higher resolution. This approach is used successfully in other studies [23,24].

A total of 6 cases are simulated. For each case, inlet velocity remains constant at 10 m/s and the rotational speed is between 3.3 and 20 rad/s for a constant tip-speed ratio (TSR) in the range of 1–6. The two-dimensional CFD power coefficients, c_p, are similar to the results of [16]. The definitions of TSR and c_p are shown in Eqs. (1) and (2), respectively, where ω is the angular speed of the turbine, R is the turbine radius, U_∞ is the freestream speed, P_T is the turbine power, ρ is the density of air, and A is the swept area of the turbine. The turbine power is calculated as the number of blades multiplied by the average tangential force of the blades, the turbine radius and the angular speed:

$$\mathrm{TSR} = \frac{\omega R}{U_\infty}, \tag{1}$$

$$c_\mathrm{p} = \frac{P_\mathrm{T}}{\frac{1}{2}\rho A U_\infty^3}. \tag{2}$$

3 Energy-based iteration scheme for the DMS model with flow expansion

3.1 Formulation

The one-dimensional, frictionless and steady flow EB-DMSM uses the flow expansion of [14]. A diagram of a streamtube is shown in Fig. 3. The energy balance in the upstream half is shown in Eq. (3), where U_∞ is the freestream speed, $\dot{m}$ is the mass flow rate, U_e is the wind speed at the equilibrium position ($x = 0$), and $\Delta\dot{W}_\mathrm{u}$ is the power extracted from the wind in the upstream half. The energy balance in the downstream half is shown in Eq. (4), where U_w is the wind speed at the wake and $\Delta\dot{W}_\mathrm{d}$ is the power extracted from the wind in the downstream half. Note that this is an energy balance per unit time (power). The upstream and downstream powers are calculated from Eqs. (5) and (6), where N is the number of blades, ω is the turbine angular speed,

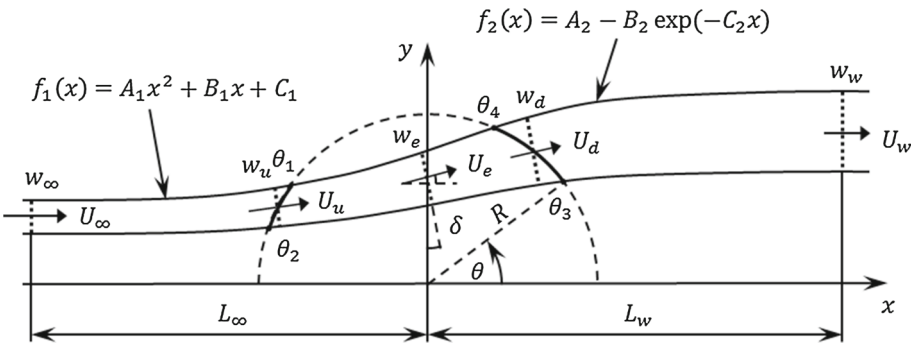

Fig. 3 Diagram of the streamtube expansion representation used in the present work, showing the mathematical representation of streamlines, velocities and streamtube widths for the energy-based and momentum-based DMS models

$\theta_1, \theta_2, \theta_3$ and θ_4 are the angular limits of the streamtubes, and F_θ is the tangential force acting on a blade. The tangential force is calculated from Eq. (7), where c is the blade chord, s is the blade span, W is the relative wind speed, c_L is the lift coefficient, c_D is the drag coefficient, and α is the angle of attack. The variables W and α are defined in Eqs. (8) and (9), respectively. The blade Reynolds number, Re_B, is defined in Eq. (10), where ν is the kinematic viscosity of air. The tangential force coefficient is defined in Eq. (11). The upstream and downstream interference factors are defined according to [14], as shown in Eqs. (12) and (13):

$$\frac{1}{2}\dot{m}U_\infty^2 - \frac{1}{2}\dot{m}U_\mathrm{e}^2 = \Delta\dot{W}_\mathrm{u}, \tag{3}$$

$$\frac{1}{2}\dot{m}U_\mathrm{e}^2 - \frac{1}{2}\dot{m}U_\mathrm{w}^2 = \Delta\dot{W}_\mathrm{d}, \tag{4}$$

$$\Delta\dot{W}_\mathrm{u} = \frac{N\omega R}{2\pi}\int_{\theta_1}^{\theta_2} F_\theta(\theta)\,\mathrm{d}\theta, \tag{5}$$

$$\Delta\dot{W}_\mathrm{d} = \frac{N\omega R}{2\pi}\int_{\theta_3}^{\theta_4} F_\theta(\theta)\,\mathrm{d}\theta, \tag{6}$$

$$F_\theta = \frac{1}{2}\rho c s W^2 (c_\mathrm{L}\sin\alpha - c_\mathrm{D}\cos\alpha), \tag{7}$$

$$W = [(\omega R + U\sin\theta)^2 + (U\cos\theta)^2]^{1/2}, \tag{8}$$

$$\alpha = \mathrm{sign}(\cos\theta)\arccos\left(\frac{\omega R + U\sin\theta}{W}\right), \tag{9}$$

$$Re_\mathrm{B} = \frac{cW}{\nu}, \tag{10}$$

$$f_\theta = \frac{F_\theta}{\frac{1}{2}\rho A U_\infty^2}, \tag{11}$$

$$u_\mathrm{u} = \frac{U_\mathrm{u}}{U_\infty}, \tag{12}$$

$$u_\mathrm{d} = \frac{U_\mathrm{d}}{U_\mathrm{e}}. \tag{13}$$

3.2 Mathematical representation of streamlines

The angular limits of the streamtubes are needed for the calculations addressed above. A mathematical representation of the streamlines (streamtube limits) based on [14] is presented in this subsection. The streamline representation is divided into upstream and downstream mathematical expressions according to Eqs. (14) and (15), where A_1, B_1, C_1, A_2, B_2 and C_2 are constants that are determined for each streamline. A comparison of the time-averaged streamlines of the CFD simulations for TSR = 4 is shown in Fig. 4. Based on the flow

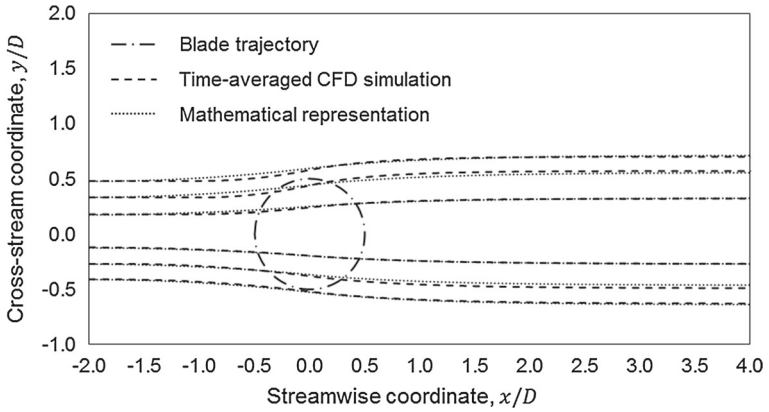

Fig. 4 Comparison of time-averaged streamlines of the two-dimensional CFD simulations and their mathematical representation based on flow expansion obtained from CFD simulations for TSR = 4

expansion of the CFD simulations, constant upstream and downstream distances, L_∞ and L_w, of two and four turbine diameters, respectively, are used for the mathematical representation. There is very good agreement between the time-averaged streamlines and the mathematical representation. The main difference is near the equilibrium position ($x = 0$), which causes slightly different curvature of the streamlines and variations in the angular limits of the streamtubes. This behavior is similar for the other tip-speed ratios studied.

Three boundary conditions are required on each half for each streamline. The upstream boundary conditions are obtained from the cross-stream coordinate of the streamline at the freestream and equilibrium positions, y_∞ and y_e, respectively, and by imposing a zero derivative at the freestream position. The downstream boundary conditions are obtained from the cross-stream coordinate at the equilibrium and wake positions, y_e and y_w, respectively, and by forcing the derivatives of f_1 and f_2 equal at $x = 0$. Note that the cross-stream coordinate at the wake is reached asymptotically, which guarantees a zero derivative of the streamline at the wake. The expressions for the constants are shown in Eqs. (16) and (17). This approach avoids the possible non-physical behavior observed with higher-order polynomials. In this case, a fourth-order polynomial would be required to cover the upstream and downstream halves because of the five boundary conditions required in that case (three cross-stream coordinates at the freestream, equilibrium and wake locations and two zero derivatives at the freestream and wake locations). Note that the streamlines are constructed sequentially from an undistorted streamline that coincides with the x axis. Thus, the left and right sides (considered from the streamwise direction) are calculated independently.

$$f_1(x) = A_1 x^2 + B_1 x + C_1, \tag{14}$$

$$f_2(x) = A_2 - B_2 \exp(-C_2 x), \tag{15}$$

$$\begin{pmatrix} A_1 \\ B_1 \\ C_1 \end{pmatrix} = \begin{pmatrix} \frac{y_\mathrm{e} - y_\infty}{L_\infty^2} \\ \frac{2(y_\mathrm{e} - y_\infty)}{L_\infty} \\ y_\mathrm{e} \end{pmatrix}, \tag{16}$$

$$\begin{pmatrix} A_2 \\ B_2 \\ C_2 \end{pmatrix} = \begin{pmatrix} y_\mathrm{w} \\ y_\mathrm{w} - y_\mathrm{e} \\ \frac{2(y_e - y_\infty)}{L_\infty (y_\mathrm{w} - y_\mathrm{e})} \end{pmatrix}. \tag{17}$$

4 Results and discussion

The EB-DMSM described in the previous section is programmed in MATLAB. The subsonic lift and drag coefficients used to obtain the tangential force are from [25]. The blade Reynolds number and the angle of attack are used to interpolate the data. The dynamic stall phenomenon observed at low tip-speed ratios [26] is included in the model through the Massachusetts Institute of Technology (MIT) dynamic stall model [27]. A sensitivity analysis is performed to study the influence of the number of streamtubes on the model performance. The best results are obtained for values between 6 and 30 streamtubes. The number of streamtubes (NST) close

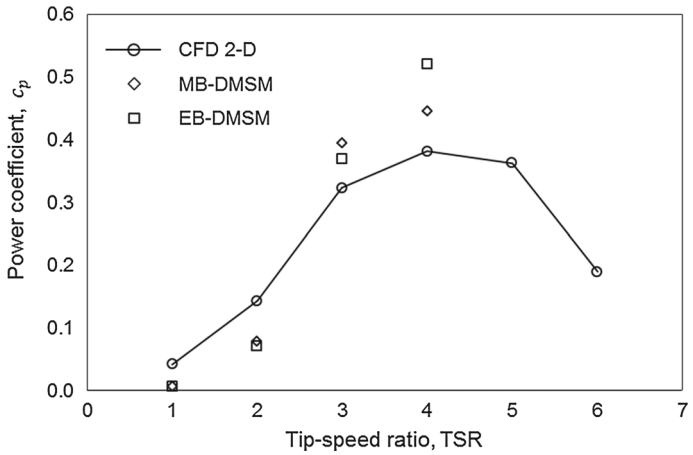

Fig. 5 Power coefficient versus tip-speed ratio comparison, two-dimensional CFD simulations, momentum-based DMS model and energy-based DMS model

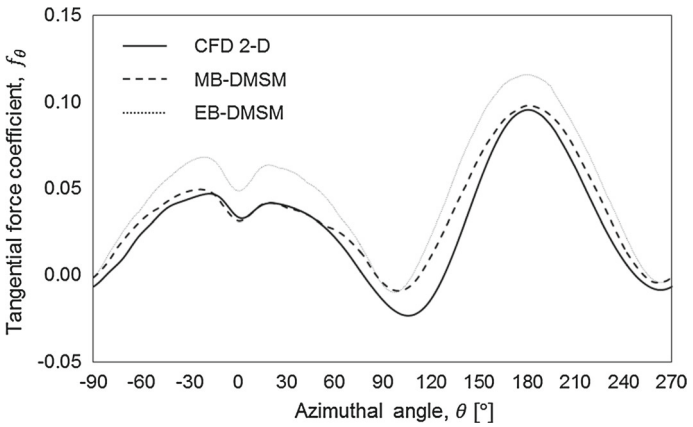

Fig. 6 Tangential force coefficient versus azimuthal angle comparison for TSR = 4, two-dimensional CFD simulations, momentum-based DMS model and energy-based DMS model

to 10 is a common value for DMS models [11,14,28]. An NST equal to 12 is used for this study because it is fast and accurate. No flow reversal is observed in the CFD simulations for the cases studied. Therefore, the equations addressed in the previous section are solved for interference factors ranging from 1.0 to 0.5. The interference factors resulting in equal left and right sides of the upstream and downstream equations, Eqs. (3) and (4), are chosen as the solution. A discretization of 0.005 was used in the interference factor. The tower effects are included using the speed deficit of [27].

To compare the accuracy of the power performance prediction of the EB-DMSM, the MB-DMSM is also implemented. The same mathematical representation for the streamlines is used. Therefore, the linear momentum equations of the MB-DMSM are very similar to the expressions used in [14]. The main difference is that in this approach the lateral expansion of the flow is considered through the angle δ. The power coefficients of the EB-DMSM, MB-DMSM and the CFD simulations are shown in Fig. 5 as a function of the TSR. The maximum differences in the peak power coefficient predictions are 16 and 32 % for the MB-DMSM and the EB-DMSM, respectively. A comparison of the tangential force coefficient of one blade is shown in Fig. 6 for TSR = 4. In general, the MB-DMSM tangential force coefficient results more closely match the CFD results.

Both models achieved convergence for tip-speed ratios up to 4. The reason convergence is not achieved for higher TSRs is that the left (one-dimensional momentum or energy balance) and right (streamwise or tangential coefficients) sides of the dimensionless EB-DMSM and MB-DMSM equations are not equal for any interference factor in the range 0.5–1, as shown in Fig. 7. This is because the aerodynamic coefficients and the dynamic stall model do not accurately represent the aerodynamics of the blades [26,29,30]; in fact, according to Fig. 6, they are overpredicted.

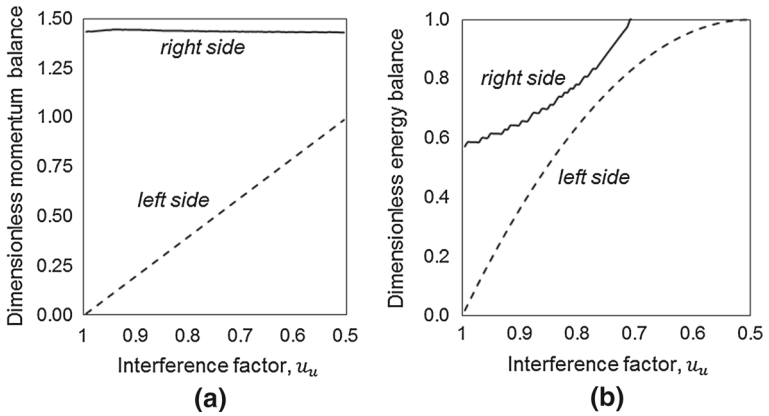

Fig. 7 Convergence issues at the first left-side streamtube in the streamwise direction for TSR = 5 and NST = 12: **a** momentum-based DMS model and **b** energy-based DMS model

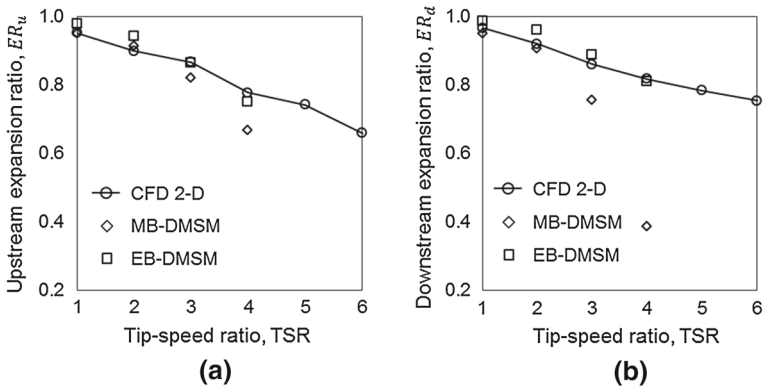

Fig. 8 Expansion ratio of the two-dimensional CFD simulations, momentum-based DMS model and energy-based DMS model: **a** upstream half and **b** downstream half

The prediction of the flow expansion is quantified through the upstream and downstream expansion ratios, ER_u and ER_d, which are defined in Eqs. (18) and (19) according to [14], where W_∞, W_e and W_w are the widths of the streamtubes that pass through the turbine at the freestream, equilibrium and wake locations, respectively. The expansion ratios of the time-averaged flow of the CFD simulations is presented for all tip-speed ratios in Fig. 8. The expansion ratios of the EB-DMSM and MB-DMSM are also shown. The flow expansion prediction accuracy decreases with increasing TSR, especially for the MB-DMSM. The maximum differences in the flow expansion prediction are 52.7 and 4.9 % for the MB-DMSM and EB-DMSM, respectively.

$$\mathrm{ER_u} = \frac{W_\infty}{W_\mathrm{e}} \tag{18}$$

$$\mathrm{ER_d} = \frac{W_\mathrm{e}}{W_\mathrm{w}} \tag{19}$$

The inability of the models to predict the power performance and flow expansion is attributed to the simplicity of the models. The one-dimensional, steady flow and frictionless theory behind the MB-DMSM and EB-DMSM is not capable of representing the complex fluid dynamics of the VAWTs.

To quantify the inaccuracy of the models, the imbalance of momentum and energy are calculated using the aerodynamic coefficients and flow expansion from the CFD results. The dimensionless quantity needed to satisfy the equations is calculated in each case as a function of the azimuthal position of one blade and the TSR, as shown in Fig. 9. The dimensionless momentum correction, MC, is the term that must be added to the left side of the equation to balance it. Hence, it can be interpreted as an additional force acting on the control volume, for instance a force caused by the unsteady flow. The dimensionless energy correction, EC, is the term that must be added to the right side of the equation. Therefore, it can be interpreted as an energy loss. The

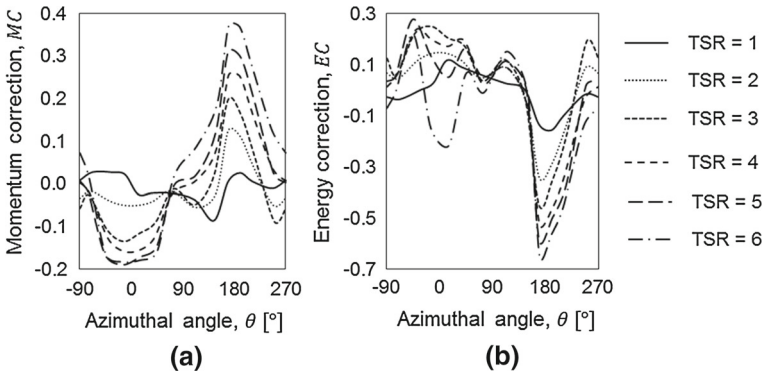

Fig. 9 Corrections as a function of the azimuthal angle and TSR imposing aerodynamic coefficients and flow expansion from CFD results: **a** momentum-based DMS model and **b** energy-based DMS model

corrections follow a pattern in both cases. The amplitude of the corrections increases with increasing TSR. Corrections are higher at the turbine center position ($\theta = 180°$ and $\theta = 0°$), which coincides with the higher blockage of the blades on the flow.

5 Conclusions

A two-dimensional energy-based iteration scheme of the DMS model (EB-DMSM) is shown in the present work. Expansion of the flow is included in the model through a mathematical representation of streamlines, which is divided into upstream and downstream halves. This new approach is compared with a momentum-based iteration scheme (MB-DMSM) and the results of a two-dimensional computational simulation of a 12-kW straight-bladed VAWT. The mathematical representation of streamlines used for modeling the flow expansion is in good agreement with simulations. Convergence of both schemes is achieved for tip-speed ratios (TSRs) up to 4. Failure of the models to convergence at higher TSRs is attributed to their inability to adequately represent the aerodynamic forces acting on the blades. The inaccuracy of both schemes is quantified using aerodynamic coefficients and flow expansion from the computational simulations. The maximum differences in the peak power coefficient predictions are 16 and 32 % and in the flow expansion predictions are 53 and 5 % for the MB-DMSM and EB-DMSM, respectively. In conclusion, EB-DMSM provides a better prediction of flow expansion, though the power prediction is not as accurate relative to MB-DMSM. The EB-DMSM would be useful for the prediction of interference among VAWTs in a wind farm. Corrections are required to improve the predictions of power performance and flow expansion of turbines with different geometric and operational parameters.

Acknowledgments The authors are grateful to Mr. Celso Rangel for providing the files of the computational domain, mesh and solution configurations that are used in the present work. Mr. Wendler would also like to thank the Comisión Nacional de Investigación Científica y Tecnológica CONICYT-PCHA/Magíster Nacional/2013-221320449 of the Chilean government for fellowship support.

References

1. Islam, M., Ting, D.S.K., Fartaj, A.: Aerodynamic models for Darrieus-type straight-bladed vertical axis wind turbines. Renew. Sustain. Energy Rev. **12**, 1087–1109 (2008)
2. Bhutta, M.M.A., Hayat, N., Farooq, A.U., Ali, Z., Jamil, S.R., Hussain, Z.: Vertical axis wind turbine—a review of various configurations and design techniques. Renew. Sustain. Energy Rev. **16**, 1926–1939 (2012)
3. Mertens, S., Kuik, G.van , Bussel, G. van : Performance of an H-Darrieus in the skewed flow on a roof. J. Sol. Energy Eng. **125**, 433–440 (2003)
4. Balduzzi, F., Bianchini, A., Carnevale, E.A., Ferrari, L., Magnani, S.: Feasibility analysis of a Darrieus vertical-axis wind turbine installation in the rooftop of a building. Appl. Energy **97**, 921–929 (2012)
5. Jamieson, P.: Innovation in Wind Turbine Design. Wiley, New York (2011)
6. Whittlesey, R.W., Liska, S., Dabiri, J.O.: Fish schooling as a basis for vertical axis wind turbine farm design. Bioinspir. Biomim. **5**, 035005 (2010)

7. Dabiri, J.O.: Potential order-of-magnitude enhancement of wind farm power density via counter-rotating vertical-axis wind turbine arrays. J. Renew. Sustain. Energy **3**, 043104-1 (2011)
8. Kinzel, M., Mulligan, Q., Dabiri, J.O.: Energy exchange in an array of vertical-axis wind turbines. J. Turbul. **13**(38), 1–13 (2012)
9. Meyers, J., Meneveau, C.: Optimal turbine spacing in fully developed wind farm boundary layers. Wind Energy **15**, 305–317 (2012)
10. Cervarich, M.C., Roy, S.B., Zhou, L.: Spatiotemporal structure of wind farm-atmospheric boundary layer interactions. Energy Proced. **40**, 530–536 (2013)
11. Paraschivoiu, I., Delclaux, F.: Double multiple streamtube model with recent improvements. J. Energy **7**(3), 250–255 (1983)
12. Zanon, A., Giannattasio, P., Ferreira, C.J.S.: A vortex panel model for the simulation of the wake past a vertical axis wind turbine in dynamic stall. Wind Energy **16**, 661–680 (2013)
13. Paraschivoiu, I.: Double-multiple streamtube model for Darrieus wind turbines. In: Second DOE/NASA wind turbines dynamics workshop, pp. 19–25. NASA CP-2186, Cleveland, OH (1981)
14. Paraschivoiu, I., Fraunié, P., Béguier, C.: Streamtube expansion effects on the Darrieus wind turbine. J. Propuls. **1**(2), 150–155 (1985)
15. McIntosh, S.C., Babinsky, H.: Convergence failure and stall hysteresis in actuator-disk momentum models applied to vertical axis wind turbines. J. Sol. Energy Eng. **131**, 034502-1 (2009)
16. Kjellin, J., Bülow, F., Eriksson, S., Deglaire, P., Leijon, M., Bernhoff, H.: Power coefficient measurement on a 12 kW straight bladed vertical axis wind turbine. Renew. Energy **36**, 3050–3053 (2011)
17. Castelli, M.R., Englaro, A., Benini, E.: The Darrieus wind turbine: proposal for a new performance prediction model based on CFD. Energy **36**, 4919–4934 (2011)
18. Castelli, M.R., Grandi, G., Benini, E.: Numerical Analysis of the Performance of the DU91-W2-250 Airfoil for Straight-Bladed Vertical-Axis Wind Turbine Application. World Academy of Science. Engineering and Technology, **63**, 855–860 (2012)
19. Rossetti, A., Pavesi, G.: Comparison of different numerical approaches to the study of the H-Darrieus turbines start-up. Renew. Energy **50**, 7–19 (2013)
20. Chung, T.: Computational Fluid Dynamics. Cambridge University Press, Cambridge (2010)
21. Chen, H., Patel, V.: Near-wall turbulence models for complex flows including separation. AIAA J. **26**(6), 641–648 (1988)
22. Castelli, M., De Betta, S., Benini, E.: Numerical investigation of the optimal spatial domain discretization for the 2-D analysis of a Darrieus vertical-axis water turbine. In: Proceedings of World Academy of Science, Engineering and Technology 64 (2012)
23. Beri, H., Yao, Y.: Numerical simulation of unsteady flow to show self-starting of vertical axis wind turbine using fluent. J. Appl. Sci. **11**(6), 962–970 (2011)
24. Howell, R., Qin, N., Edwards, J., Durrani, N.: Wind tunnel and numerical study of a small vertical axis wind turbine. Renew. Energy **35**(2), 412–422 (2010)
25. Sheldahl, R.E., Klimas, P.C.: Aerodynamic Characteristics of Seven Symmetrical Airfoil Sections Through 180-Degree Angle of Attack for Use in Aerodynamic Analysis of Vertical Axis Wind Turbines. Sandia National Laboratories—energy report, SAND80-2114 (1981)
26. Fujisawa, N., Shibuya, S.: Observations of dynamic stall on Darrieus wind turbine blades. J. Wind Eng. Ind. Aerodyn. **89**, 201–214 (2001)
27. Paraschivoiu, I.: Wind Turbine Design: With Emphasis on Darrieus Concept. Press Internationales Polytechnique, Montreal (2002)
28. Paraschivoiu, I., Désy, P., Masson, C.: Blade tip, finite aspect ratio, and dynamic stall effects on the Darrieus rotor. J. Propuls. **4**(1), 73–80 (1988)
29. Delnero, J.S., Marañon di Leo, J., Bacchi, F.A., Colman, J.U. Boldes: Experimental determination of the influence of turbulent scale on the lift and drag coefficients of low Reynolds number airfoils. Latin Am. Appl. Res. **35**, 183–188 (2005)
30. Bedon, G., Antonini, E.G.A., de Betta, S., Castelli, M.R., Benini, E.: Evaluation of different aerodynamic databases for vertical axis wind turbine simulations. Renew. Sustain. Energy Rev. **40**, 386–399 (2014)